Plasmid Transfection in Mammalian Cells Spatiotemporally Tracked by a Gold Nanoparticle

Megan E. Muroski, Kate J. F. Carnevale, Ryan A. Riskowski, and Geoffrey F. Strouse*

Department of Chemistry and Biochemistry, Florida State University, Tallahassee, Florida 32306-4390, United States

ABSTRACT Recent advances in cell transfection have suggested that delivery of a gene on a gold nanoparticle (AuNP) can enhance transfection efficiency. The mechanism of transfection is poorly understood, particularly when the gene is appended to a AuNP, as expression of the desired exogenous protein is dependent not only on the efficiency of the gene being taken into the cell but also on efficient endosomal escape and cellular processing of the nucleic acid. Design of a multicolor surface energy transfer (McSET) molecular beacon by independently dye labeling a linearized plasmid and short duplex DNA (sdDNA) appended to a AuNP allows spatiotemporal profiling of the transfection events, providing insight into package uptake, disassembly, and final plasmid expression. Delivery of the AuNP construct encapsulated in Lipofectamine2000 is monitored in Chinese hamster ovary cells using live-cell confocal microscopy. The McSET beacon signals the location and timing of the AuNP release and endosomal escape events for the plasmid and the sdDNA discretely, which are correlated with plasmid transcription by fluorescent protein expression within the cell. It is observed that delivery of the construct leads to endosomal release of the plasmid and sdDNA from the AuNP surface at different rates, prior to endosomal escape. Slow cytosolic diffusion of the nucleic acids is believed to be the limiting step for transfection, impacting the time-dependent expression of protein. The overall protein expression yield is enhanced when delivered on a AuNP, possibly due to better endosomal escape or lower degradation prior to endosomal escape.

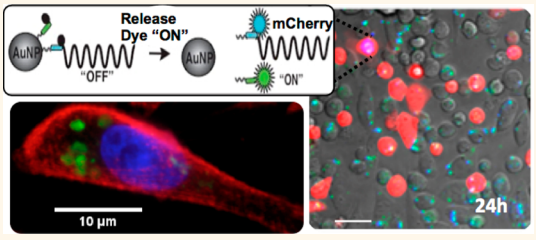

KEYWORDS: gold nanoparticle · SET · energy transfer · transfection · *in vitro* · optical imaging · molecular beacon

The development of personalized medicine for the treatment of disease states at the cellular level using cell therapy strategies is a global dream for healthcare. Exploiting the full potential of cell therapy requires the successful transfection of individual cells to induce specific changes in protein expression profiles within the cell.[1] For clinical applications of engineered cells, nonviral methods are preferred due to the drastically reduced risks of immune response following transfection of plasmid, small interfering RNA (siRNA), messenger RNA, or a combination of therapeutic agents.[2−5] However, changes in protein expression following transfection *via* nonviral protocols can be highly variable.[2,6−16] The variability in protein expression is believed to reflect endosomal sequestration which leads to subsequent nucleic acid damage and thus reduced levels of exogenous protein expression.[17−20] The nucleic acid damage reflects an inability to escape the endosome, resulting in degradation from rising reducing agent levels and acidity within the endosomal vesicle.[21−23]

In many cases, a lipid, polymer, or other chemical agent is utilized to package the nucleic acid and enhance the cellular uptake.[24−26] Recent studies have demonstrated that gold nanoparticles (AuNPs) show promise as carriers for appended nucleic acid sequences with enhanced transfection and protein yields when packaged in liposomes.[27−29] The improvement in protein yields has been hypothesized to be due to reduced endosomal degradation of the nucleic acid.[14,15,21,30−37] Connecting the improved transfection yields with the cellular processing of the delivered agents requires detailed insight into the important steps for transfection when using a AuNP delivery agent.

Critical progress in the rapidly developing field of nanotherapeutics necessitates the understanding of fundamental processes such as agent uptake, endosomal encapsulation, timing of plasmid release and

* Address correspondence to strouse@chem.fsu.edu.

Received for review August 8, 2013 and accepted December 15, 2014.

Published online December 15, 2014
10.1021/nn5060305

© 2014 American Chemical Society

subsequent protein expression, as well as the fate of the delivery agent. Whether the goal is delivery of a therapeutic drug, siRNA to interfere with endogenous protein expression, or a linearized plasmid to induce exogenous protein expression, being able to follow the progression of transfection to identify the limiting steps for successful cargo delivery and activation is important and not easily accomplished using standard biochemical methods.

In this article, we examine the limiting steps in cellular transfection of a AuNP delivery agent carrying a gene and a short DNA sequence, encapsulated in Lipofectamine2000. Liposome encapsulation allows the broader applicability of the study to be realized by the cellular biology community, as Lipofectamine2000 is a commercially available standard transfection technique. In the study, the coupling of the AuNP delivery vehicle to multicolor surface energy transfer (McSET) techniques allows the timing of release of both a linearized plasmid (4.7 kbp) and short duplex DNA sequences (35 bp) from the surface of a AuNP to be visualized. The dynamics of the events within the cell are mapped by spinning disk confocal microscopy, while locations of agents are characterized *via z*-contrast spectral confocal fluorescent microscopy. Using McSET methods, the difference in release dynamics and endosomal processing of sdDNA and a full linearized plasmid are discretely mapped in separate optical channels. The results of the study indicate that the plasmid and sdDNA release at different rates within the endosome, with the rate-limiting step being endosomal escape. The results suggest that accessibility of reducing agents to the Au–sulfur bond arising from packaging of the linearized plasmid at the AuNP surface may be critical in release but is not critical in endosomal escape. The delayed release of the plasmid relative to the short duplex DNA (sdDNA) from the AuNP leads to delayed diffusion of the plasmid into the cytosol and potentially lower expression levels. However, the transcription of the plasmid is not impacted by AuNP transfection, with mCherry expression observed within 4 h of endosomal release, consistent with expected expression rates for the fluorescent protein.

The developed McSET biophysical tracking technique is a universal tool that can give insight into the individual events of transfection by providing optical feedback on the processing of a delivered cargo from a nanoparticle transfection agent. The McSET beacon strategy allows the AuNP transfection agent to report the AuNP–plasmid release event based upon a visual "on–off" signature of the dye-labeled nucleic acids.[38,39] Several groups have utilized SET for biophysical investigations and, more recently, to verify the transfection of nucleic acids into cells when delivered on a gold nanoparticle carrier.[27,36,40–42] However, the use of spatiotemporal profiling of delivery using time lapse live-cell microscopy has not been carried out, despite the capability of McSET combined with a AuNP dual delivery agent to provide exquisite detailed information on the transfection event. The full potential of SET for imaging dynamic intracellular events, such as the release of nucleic acid sequences from the surface of a AuNP carrier, can allow therapeutically relevant intracellular events to be observed in real time, during the normal cell cycle.[43]

RESULTS AND DISCUSSION

Assembling the AuNP–DNA–Plasmid Construct. The McSET beacon uses a 6.6 nm AuNP to co-assemble a blue-labeled (DyLight350, λ_{em} = 432 nm) linearized plasmid (plasmid) and a green-labeled (DyLight488, λ_{em} = 518 nm) 35 bp sdDNA as a mimic of siRNA or antisense DNA. The choice of the DyLight dyes reflects the reported low photobleaching and lack of pH or reducing agent sensitivity.[44] The plasmid is designed to induce expression of the fluorescent protein mCherry (λ_{em} = 610 nm) intracellularly following transcription and provides correlated feedback on transfection and subsequent transcription to verify plasmid integrity following transfection. The selected wavelengths allow distinct spectral resolution within a spinning disk confocal microscope with a frame rate for imaging at $\leq$1 s averaging, collected every 0.5 h.

The McSET construct is assembled in a 50:1 ratio of 35 bp sdDNA and a 4.75 kbp plasmid on a 6.6 nm AuNP. The plasmid is coupled in a 1:1 ratio to the AuNP. Appendage of the thiol-modified nucleic acids to the surface of the AuNP, previously coated in bis(*p*-sulfonatophenyl)phenylphosphine (BSPP) protecting group, is accomplished by sequential thiol place exchange reactions where the plasmid is loaded first and then the AuNP is backfilled with the sdDNA to achieve the desired ratio, following procedures described previously for the assembly of plasmid and short DNA sequences onto AuNPs.[27,45] The actual loading level is stochastic.[27] The McSET platform was measured against controls consisting of AuNPs bound to only the plasmid, only sdDNA, co-appended plasmid with unlabeled sdDNA, co-appended unlabeled plasmid with sdDNA, and unlabeled linearized plasmid alone without the AuNP. Encapsulation of the transfection constructs into the cationic liposome, Lipofectamine2000, is performed at a concentration of 4 μg/10 μL, which produces spherical lipid-coated packages.

Formation of the McSET constructs is evidenced by changes in the gel electrophoresis (1% agarose) mobility (Supporting Information SF1). The gel electrophoresis image in Figure SF1 shows retention differences for the AuNP constructs when compared to AuNP–BSPP. The retention of mobility of the AuNP constructs implies that the plasmid dominates the mobility in the gel, likely due to the large size and charge density of the DNA. No emission from the dye labels is observed under UV illumination as expected

due to the strong SET quenching. The lack of emission is consistent with formation of a Au−S bond to the DNA and the maintenance of the construct under the electrophoretic conditions.

Empirical evidence for formation of the AuNP transfection construct can be deduced by contrasting the dynamic light scattering behavior for the AuNP−BSPP, AuNP−sdDNA, AuNP−plasmid/sdDNA, and plasmid alone (Supporting Information Figure SF2). From the dynamic light scattering (DLS) data, distinct hydrodynamic radii are observed for the AuNP−BSPP (4.2 nm), the assembled AuNP−sdDNA (17 nm), AuNP−plasmid/sdDNA construct (75 nm), and the plasmid (126 nm). The DLS measurements were carried out in nanopure water with six repeats of 10 measurements each to ensure statistical validity of the data. The hydrodynamic radius of the linearized plasmid is consistent with a 4.7 kbp sequence exhibiting a globular structure. The size of the AuNP−plasmid/sdDNA transfection construct is smaller than the free plasmid, likely reflecting compaction of the plasmid at the NP surface. The compaction arises from van der Waals and electrostatic interactions. The hydrodynamic radius is often larger than the TEM analysis for AuNPs reflecting the observed size difference reported by TEM and DLS in the literature.[46] The Lipofectamine2000-encapsulated size for linearized plasmid (538 nm), the AuNP−plasmid (372 nm), and the AuNP−sdDNA (361 nm) is measured by DLS (data not shown). The size of the liposome transfection package depends strongly on the construct composition. The formation of a stable liposome package will be influenced by differences in zeta-potential and hydrophobicity in the AuNP−DNA *versus* the AuNP−plasmid. The package size likely reflects differences in the surface charge for the different assemblies, which impacts the DLS values. The increase in Lipofectamine2000 package size for the plasmid, AuNP−plasmid, and AuNP−sdDNA is consistent with expectation.

Cellular Transfection and Nucleic Acid Release. The McSET molecular beacon toolset utilizes a AuNP and a dye molecule to observe biological events. Using time-resolved live-cell microscopy, McSET allows for inquiry into the transfection of a single cell and the direct spatiotemporal profiling of the steps of transfection to be observed in real time during the normal cell cycle. SET methods offer a distinct advantage over other optical probe techniques, not only to analyze static transfection events such as release and expression but also to obtain dynamic information about transfection as it progresses, shown schematically in Figure 1. The McSET molecular beacon provides a wavelength-specific "off−on" response that indicates location, timing, and magnitude of sdDNA *versus* plasmid release from the AuNP once endocytosed by the cell. The time-dependent changes in fluorophore intensity in the red (mCherry), green (DyLight488), and blue (DyLight350)

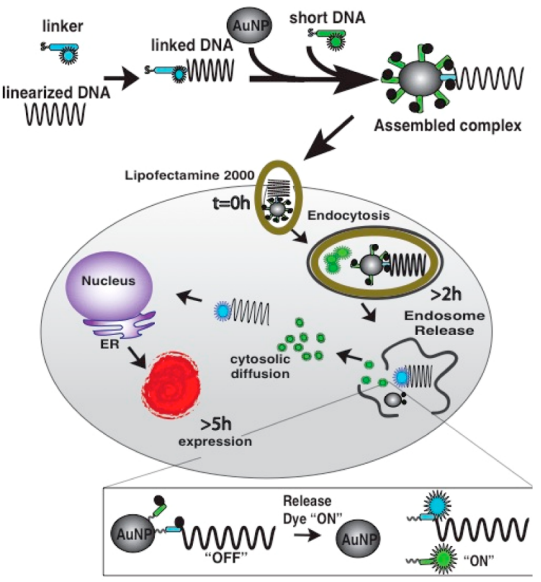

Figure 1. Schematic of AuNP transfection construct assembly, Lipofectamine encapsulation, endocytosis of the package, and cellular processing to initiate fluorescent protein production. The inserted image represents the McSET molecular beacon that allows the endosomal plasmid release from the nanoparticle surface event to spatiotemporally imaged.

channels (every 30 min for 24 h) collected using a live-cell chamber coupled to a spinning disk confocal microscope provide temporal and spatial resolution of the transfection steps. Release of the nucleic acid cargo from the AuNP surface is determined by the appearance of the appropriate dye frequency (sdDNA, green; linearized plasmid, blue), providing a snapshot of the discrete release events and spatial localization which are then analyzed over time to give dynamic information about transfection progression at the single-cell level.

The time-dependent fluorescence microscopy images in comparison to the differential image contrast (DIC) images are shown in Figure 2 at 0, 8, 12, and 24 h. Comparison of the fluorescence channels to the DIC overlay allows the boundaries of the cell to be visualized. A time-dependent increase in green and blue emission intensity arises in the imaged Chinese hamster ovary (CHO) cells over a 24 h time period. Note that the higher ratio of sdDNA to plasmid is reflected in the higher green intensity in Figure 2. The appearance of green emission signals sdDNA release, while blue indicates release of the plasmid from the AuNP. Inspection of video capture in Supporting Information SF3 shows that the initial packages are "off", and slow continuous appearance of emission occurs once packaged within the cell. The lack of intensity outside the cell boundaries indicates that no release occurs prior to cell uptake. The observation of emission once endocytosed implies that sdDNA and plasmid release occur within the endosomal package, presumably reflecting the change in pH and reducing environment for the package as the endosome matures.

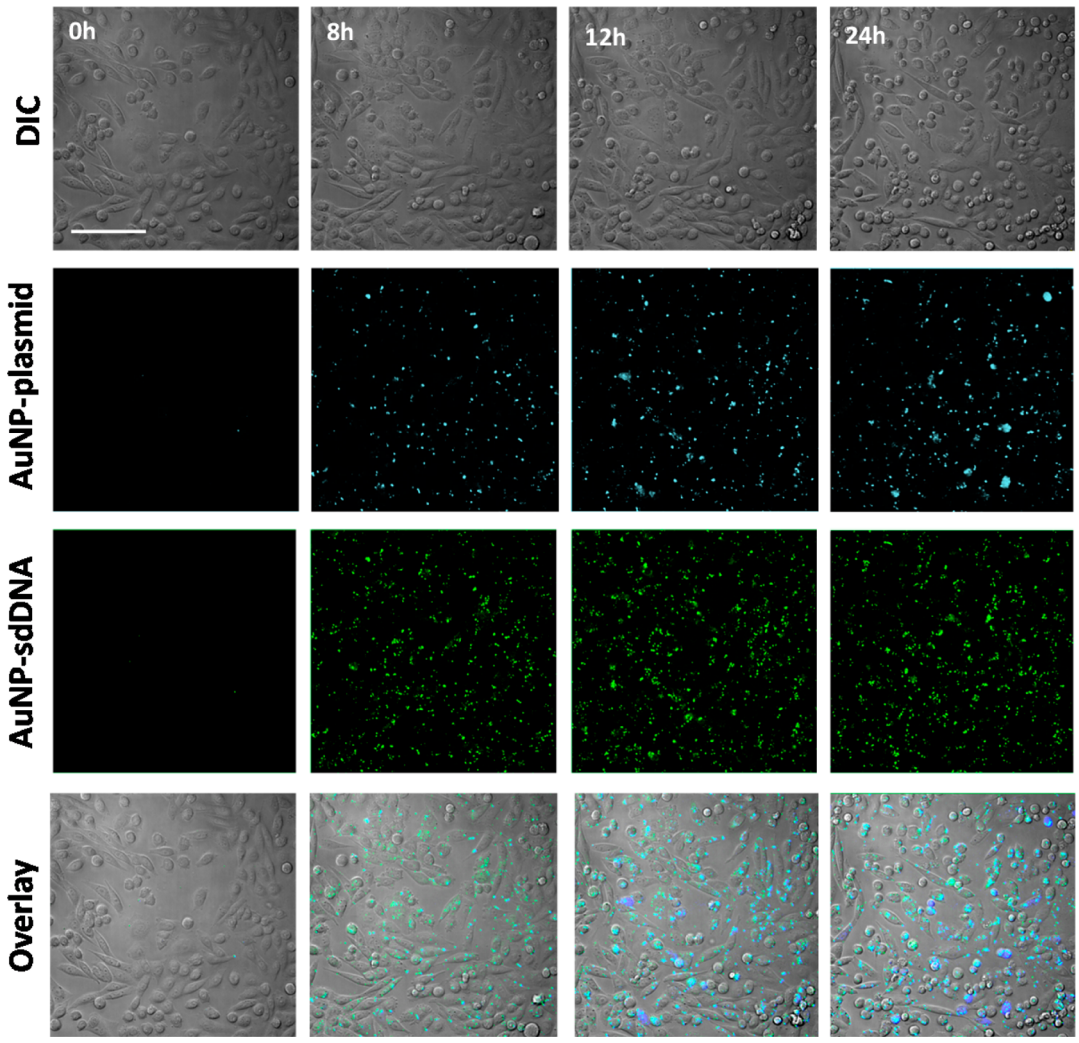

Figure 2. Live-cell, wide-field microscopy imaging (20×) in CHO cells plated at 30 000 cells/cm^2 at t = 0, 8, 12, and 24 h following transfection by the AuNP−plasmid/sdDNA in (a) DIC, (b) fluorescence from Dylight350, plasmid linker dye, (c) fluorescence from Dylight488, short duplex DNA dye. The wide-field images (20× magnification, scale bar = 50 μm) are collected under 405 nm excitation (1 s) and 488 nm excitation (300 ms exposure) for (b) and (c), respectively.

Spatial Distribution. In addition to changes in intensity, the spatial distribution changes from strongly punctate to diffuse within the cell. The observation of the increasing emission within punctate packages in time is indicative of endosomal packaging of the transfected agent. The endosomal packaging is consistent with models for nanoparticle uptake into cells *via* endosomal pathways. The punctate pattern is time-dependent with increasing spot size reflecting endosomal repackaging. Diffusion of the emission across the entire cell at later times indicates cytosolic diffusion of the delivered agent. No evidence of exocytosis is observed within the 24 h time frame of the experiment. The appearance of emission with a punctate pattern over similar time scales is observed for the dye-labeled AuNP−sdDNA and AuNP−plasmid controls, as well (Supporting Information SF4).

The optical images in Figure 2 indicate that the sdDNA and the plasmid remain bound to the AuNP during Lipofectamine2000 transfection. Release of the plasmid and the sdDNA appear to occur within the endosomal packages with evidence of time-dependent repackaging. Slow endosomal escape with cytosolic diffusion occurs, indicative of the endosomal escape being the slow step in the transfection process.

Temporal Dynamics. The temporal dynamics of release can be extracted from the time-dependent data in the videos in Supporting Information by taking the green and blue intensity at each time point corrected for cell count. To predict the behavior, it is instructive to write the process in terms of a set of discrete steps, each with a rate (Scheme 1).

In the scheme above, LGD is the liposome−gold−dye complex, GD represents dye still appended to the gold nanoparticle, and D* represents the emitting dye once released from AuNP surface in which the subscript "endo" refers to endosomally localized and "cyto" refers to dye dispersed in the cytosol. Only k_3 and k_4 are experimentally observable by the "on" event for the molecular beacon as k_1 and k_2 will take place in

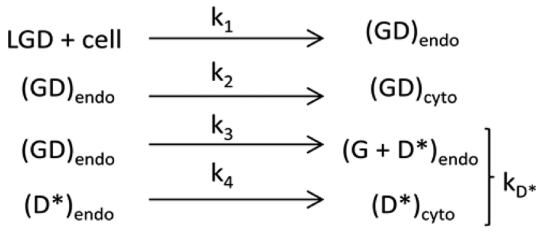

Scheme 1. Simplified reaction mechanism for dye release from AuNPs following endocytosis of the transfection platform.

the dyes' "off" state and therefore not be measurable. Solving for the kinetics of dye onset predicts a first-order rate behavior for dye turn-on; if we do not distinguish between events 3 and 4, the average release rate can be extrapolated (k_{D^*}). Plots of the time-dependent normalized (I/I_{max}) intensity of the blue (plasmid) and green (sdDNA) channels for the microscopy images corrected for cell count are shown in Figure 3. Fitting the points reveals a rate for turn-on of k_{D^*} (sdDNA) = 0.204 h^{-1} and of k_{D^*} (plasmid) = 0.063 h^{-1}. The 95% CL for the rates are 0.0156 (sdDNA) and 0.0092 (plasmid). The R^2 values are 0.994 (sdDNA) and 0.995 (plasmid). The results of the kinetics study indicate that release of the sdDNA *versus* plasmid from the AuNP surface occurs on different time scales, with the sdDNA exhibiting a greater than 2-fold faster rate. Statistical analysis using the unpaired student *t* test reveals that the events are statistically significant ($p = 0.0002$).

Onset of Exogenous Protein Expression. Endosomal release of the plasmid from the AuNP as implied by the appearance of dye emission does not necessarily translate to efficient protein expression in the CHO cells since expression can only occur if an intact plasmid migrates out of the endosome and is processed by the cell. Comparing the time-dependent evolution of red emission and percentage of cells that express mCherry (red) emission provides the necessary insight into the total transfection process within the CHO cells. In Figure 4A, the fluorescence microscopy images for mCherry expression for the AuNP−plasmid/sdDNA and plasmid alone are shown at 0, 12, and 24 h. Control sequences in which one of the nucleic acid sequences is unlabeled or absent are shown in Supporting Information SF4. It is clear from the image that the plasmid alone exhibits low expression.

In Figure 4B, the percentage of cells exhibiting red fluorescent protein expression over time are plotted for the AuNP−plasmid/sdDNA construct and controls. The percent expression can be fit to a sigmoid curve reflecting the onset and rise in mCherry protein expression. The curves yield a half-life and percent cell expression of 13.0 h (47.9% ± 3.03) for the dual-labeled AuNP−plasmid/sdDNA construct, 12.4 h (49.3% ± 1.41) for the AuNP-unlabeled plasmid/labeled sdDNA, 13.0 h (54.6% ± 4.70) for AuNP-unlabeled plasmid, and

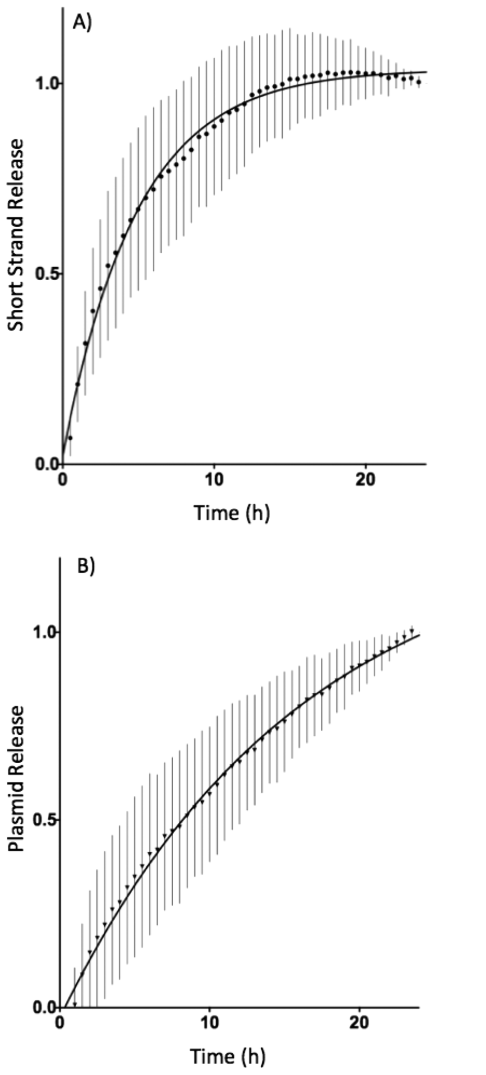

Figure 3. Kinetics plot of the normalized intensity per cell for dye release collected at 30 min intervals for AuNP−plasmid/sdDNA over 24 h. The data are fit to $I(t) = I_0\exp(-kt)$.

20.6 h (32.8% ± 2.64) for plasmid alone. Comparison of the protein expression half-life to the release kinetics reveals approximately a 3 h half-life for protein expression following release. The dynamics for mCherry expression are corrected for cell count.

It is clear that the AuNP does not delay plasmid expression and may actually result in enhancement of plasmid expression by providing a more effective endosomal escape of intact plasmids or a protective environment within the endosome as suggested by Mirkin *et al.*[15] Furthermore, the statistically indistinguishable percentage of expressing cells for AuNP−plasmid/sdDNA and the control AuNP−plasmid indicates no observed influence of the short DNA sequence or dye labeling on the yield of plasmid expression for the data in Figure 4. The experimental observation of transfection by the Lipofectamine2000-encapsulated plasmid by standard transfection protocols leading to delayed and lower level expression of

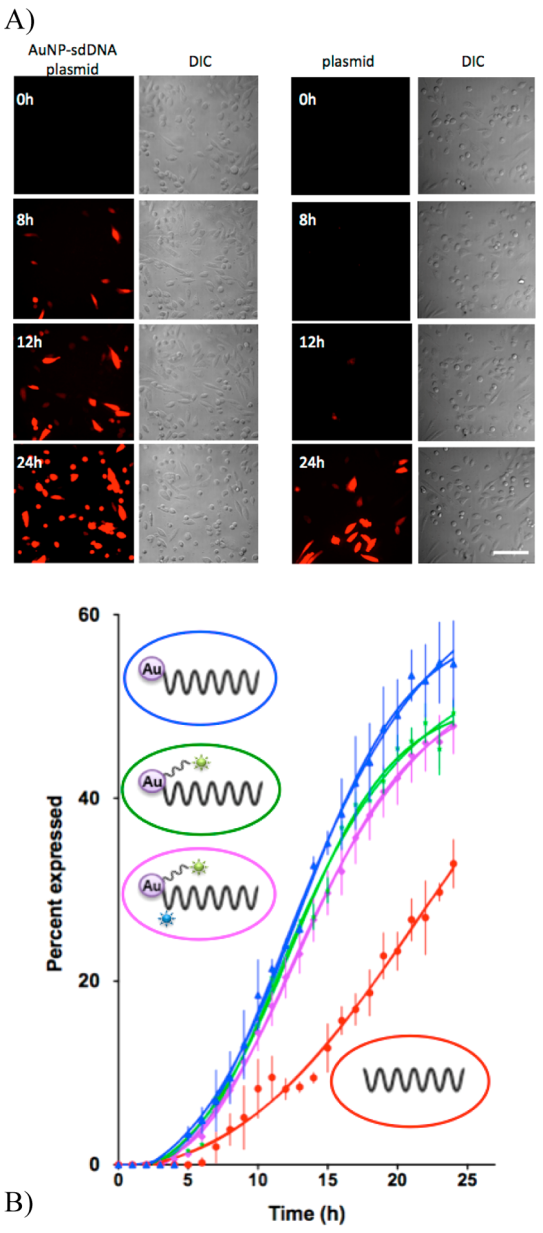

Figure 4. (A) Confocal microscopy image (20×) showing the red channel at 0, 12, and 24 h for the transfected CHO cells (scale bar = 50 μm). (B) Percent cell expression of mCherry in CHO cells over time. The data are fit to a sigmoidal function. For the AuNP−plasmid with the sdDNA appended with and without plasmid dye (♦ and ★), the AuNP−plasmid without the sdDNA appended (▲), and the linearized plasmid without an appended AuNP (●). The transfections were carried out in Lipofectamine2000 for all samples on CHO cells plated at 30 000 cells/cm^2.

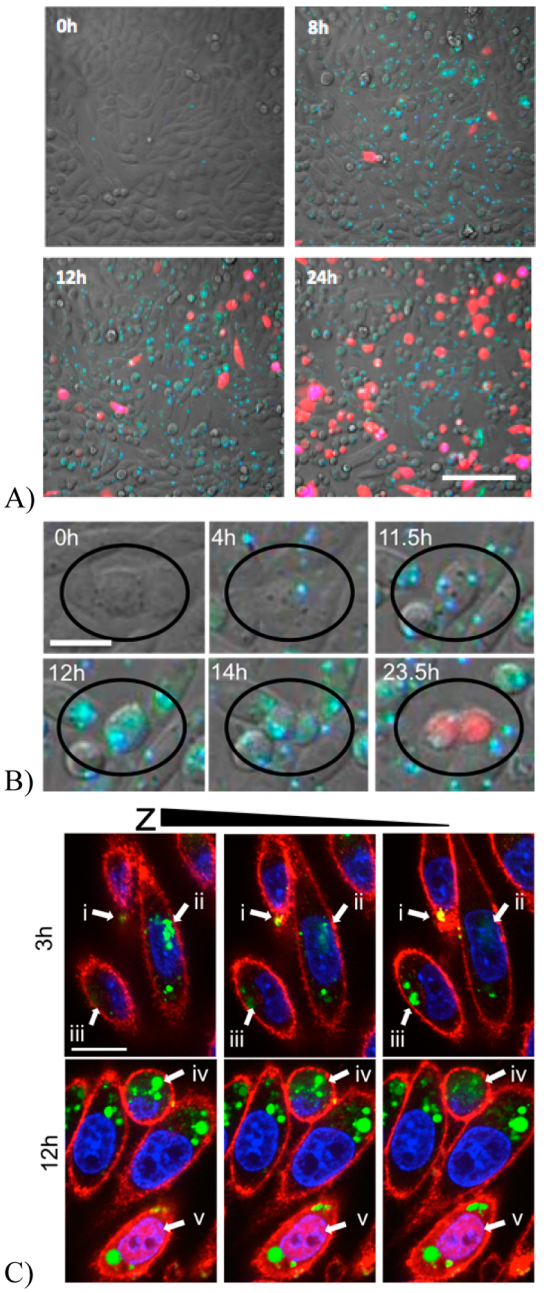

Figure 5. (A) Wide-field images (20×, scale bar = 50 μm) at 0, 8, 12, and 24 h of AuNP−plasmid/sdDNA transfected cells showing DNA release and protein expression. (B) Digitally zoomed images (20×, scale bar = 10 μm) at selected time points showing endosomal repackaging of the gene following mitosis, gene diffusion out of the endosomal package, and gene expression for a single cell. (C) Selected *Z*-stack slices imaged by confocal microscopy at 60× (scale bar = 10 μm), demonstrating (i) membrane association, (ii) nonnuclear localization, (iii) endosomal encapsulation, (iv) cytosolic diffusion, and (v) mCherry expression.

mCherry when compared to the AuNP−plasmid construct is intriguing. The difference in protein expression level is not due to AuNP, plasmid, liposome, or concentration differences, based on negligible cytotoxicity. The difference is believed to potentially reflect a larger fraction of degraded plasmid for Lipofectamine2000-delivered *versus* AuNP-delivered plasmid, consistent with the suggestion that loading of nucleic acid sequences onto a AuNP leads to decreased degradation within the cell.[47] The selected time points are a representation, and the videos show that the events occur stochastically (Supporting Information SF3).

Location, Repackaging, and Fate of Transfection Constructs. In Figure 5A, the global confocal images at 0, 8, 12, and 24 h for the red, green, and blue channels are shown. In the microscope images, it is clear that colocalization of

the green and blue dyes is observed within endosomal packages and the cytosol. As the mCherry is expressed, the appearance of purple reflects the combination of red, green, and blue in the cell. At the cell level, further insight into the transfection and repackaging events can be gained. In Figure 5B, the release of the plasmid is visualized *via* the blue dye turn-on at 4 h as well as release of the sdDNA with the green dye. In the following cell division, the packages are observed to split between the daughter cells at 14 h, with subsequent mCherry expression at 23.5 h. The observed repackaging results in enhanced transfection yield reported in our earlier paper.[27]

The location of the endosomal packages within the cell can be spatially resolved using *Z*-contrast confocal imaging. Cells transfected with AuNP-unlabeled plasmid/sdDNA, then stained with WGA-594 surface membrane stain and DAPI nuclear stain are shown in Figure 5C. As the images proceed along the *Z*-direction, from the top of each cell to its base, various events can be observed that verify DNA release occurring during endosomal encapsulation, followed by cytosolic diffusion and mCherry gene expression. Figure 5C-i demonstrates that the endocytosed packages near the base of the cell associate with the plasma membrane at 3 h, resulting in the observed overlap of red and green channels producing a yellow signal due to colocalization. The yellow color is not visible at higher *Z*-positions in the cell. Non-nuclear localization of punctate endosomally encapsulated packages is observed as green packages and can be seen above the nucleus but not in the plane of the nucleus (5C-ii). Additionally, punctate endosomally encapsulated packages can be seen at lower depths of the cell (5C-iii); at 12 h, both punctate endosomal encapsulation as well as diffuse cytosolic escape can be observed at different *Z*-depths (5C-iv). Expression of mCherry can be observed at 12 h throughout all *Z*-depths by diffuse red in the cytosol and red/blue (purple) over the nucleus due to colocalization with the DAPI nuclear stain (5C-v). The purple colocalization allows for differentiation of the mCherry from the red membrane stain, which does not colocalize with the cytosol or nucleus as observed in the other cells of the 12 h image (5C-v *vs* 5C-iv).

CONCLUSION

By utilizing biophysical tools, including Lipofectamine2000-assisted AuNP transfection, fluorescent protein expression, and the McSET live-cell beacon, the complete transfection cycle following treatment by a AuNP transfection construct can be dynamically visualized in live cells. The experimental results map the steps of the cell transfection process and confirm that endocytosis of a AuNP transfection agent leads to rapid plasmid release, plasmid translocation, and eventual efficient plasmid expression. The slow step of the process appears to be the unpackaging of the plasmid from the AuNP surface. Following plasmid unpackaging within the endosome, the plasmid is released from the AuNP surface and diffuses into the cytosol. The experimental results indicate that a slow but continuous release process occurs within the cell. The observed slow endosomal escape and cytosolic diffusion within the molecular beacon study is consistent with the suggestion that endosomal rupture leading to endosomal escape of the intact plasmid is the crucial step to ensure efficient plasmid expression following transfection.[12,21,23]

Optically mapping the nonviral transfection of nucleic acids delivered on a AuNP in real time allows for elucidation of both the release rates from the particle surface as well as the timing and efficiency of protein expression within the cell. The observation that plasmid transcription levels are not influenced by the co-assembly of a short DNA sequence onto the AuNP suggests that a plethora of plasmid-regulating agents could be simultaneously delivered by co-assembly approaches onto the AuNP surface. Understanding the parameters that effect efficient transfection and subsequent genetic manipulation of cells will have an important impact in the generation of biomedically relevant cell therapeutics.

METHODS

Materials. Water-soluble, spherical 6.6 nm AuNPs were synthesized by standard literature protocols for aqueous AuNP citrate nanoparticles.[48] Briefly, a sparged aqueous solution of tetrachloroauric acid hydrate (Strem Chemicals) was reduced in the presence of citric acid and tannic acid (Sigma) at 60 °C with rapid stirring at a ratio of 1:4:0.5 mL of each 1% (by mass) solution in 100 mL of H_2O total volume. The prepared AuNPs were exchanged with bis(*p*-sulfonatophenyl)phenylphosphine (Sigma) as the protecting group. Stoichiometric displacement of the coordinated BSPP passivation layer is accomplished by thiol place exchange reactions using 5′-thiol-terminated DNA sequences, as described previously.[27] The synthetic plasmid linker and sdDNA sequences are purchased from Midland Oligos and are listed in Supporting Information.

Preparation of AuNP–sdDNA. AuNP–sdDNA was prepared by complete thiol place exchange of the BSPP passivation layer using a 5′-C_6-thiol-terminated sdDNA. The sdDNA consisted of a synthetic 35 bp sequence containing a 5′-C_6 thiol and an internal dye label incorporated at the 30th bp through an internal modification of the T base. The exchange was carried out in a 50:1 mol ratio of sdDNA to AuNP, resulting in displacement of ~50 passivating sites on the AuNP surface. The loading of the sdDNA was confirmed by melting studies. Gel electrophoresis (2% agarose) indicated a single red band that was retained stronger than the AuNP–BSPP, consistent with formation of AuNP–sdDNA.

Preparation of AuNP–Plasmid and AuNP–Plasmid/sdDNA Constructs. The AuNP–plasmid and AuNP–plasmid/sdDNA constructs were prepared by initial assembly of a linearized plasmid,

appended to a linker sequence (with or without DyLight350 internal labeling), to the AuNP surface by thiol place exchange. To achieve co-assembly, the sdDNA (with or without DyLight488 labeling) was then back-loaded at a 50:1 ratio to the AuNP−plasmid in the presence of reducing agent, tris(2-carboxyethyl)phosphine (Sigma). The dye labels for each sequence were located on the 30th bp from the terminal thiol modification *via* an internal labeling of the T base.

The linker-modified plasmid was prepared using a commercially available mCherry-C1 plasmid (Clontech) digested with PCII (New England Biolabs (NEB)) following the manufacturer's protocol. The plasmid contained a CMV promoter to ensure overexpression of the fluorescent protein within the cell following the translation of the delivered plasmid. The digested plasmid (single cut site) was analyzed on a 1% agarose gel to validate digestion. A synthetic sdDNA linker strand (35/39 bp) containing a 4 bp overhang and a protected 5′-C_6 thiol modification to the phosphate backbone was ligated to the linearized plasmid by standard T4 ligation methods (NEB). The sequences are available in Supporting Information. The ligated plasmid containing the chemically protected C_6 thiol spacer was precipitated by addition of EtOH and stored at 4 °C. Isolation of the linearized DNA was verified by UV−vis analysis of the 260 nm absorption for DNA.

The protected thiol plasmid was appended to the AuNP through formation of a AuNP−sulfur bond followed by stoichiometric thiol place exchange reactions in a 1.1:1 plasmid to AuNP ratio. The AuNP−plasmid construct was achieved by initial deprotecting of the thiol plasmid through treatment with reducing agent dithiothreitol (20 mM, 2 h, RT). The deprotected plasmid was then passed through a NAP-5 (Sephadex G-25 DNA grade) gravity flow size exclusion column following the manufacturer's protocol to isolate the deprotected linearized plasmid from the reducing agent and the free protecting group. The deprotected thiol on the plasmid reacts with the AuNP surface (stable for ∼30 min at RT). Coupling of the plasmid to the AuNP surface was carried out by addition of the deprotected plasmid to a solution containing the AuNP and allowed to place exchange for 48 h. The assembled AuNP−plasmid was pelleted out of solution by centrifugation at 3000 rpm to remove unbound plasmid. Co-assembly of the sdDNA (dye-labeled or unlabeled) onto the AuNP−plasmid construct was carried out by backfilling, following the protocol described previously to dual label a AuNP with separate nucleic acid sequences.[27] Briefly, a 50:1 ratio of reduced thiol sdDNA was added to the AuNP−plasmid construct. Gel electrophoresis (1% agarose) of the AuNP−plasmid construct confirmed assembly and showed <1% free AuNP present.

Transfection Agent. The AuNP transfection construct was prepared by encapsulating AuNP−sdDNA, AuNP−plasmid, or AuNP−plasmid/sdDNA into Lipofectamine2000 (Life Technologies). Lipofectamine2000 encapsulation of the AuNP constructs was carried out at a concentration of 4 μg of DNA agent to 10 μL of Lipofectamine2000. The loading level of constructs into the liposome was chosen to be consistent with concentrations utilized in the protocol for a standard plasmid transfection in Lipofectamine2000.[49] Dynamic light scattering data (DynaPro-Titan) was obtained at 20% laser power and used to analyze the size of the transfection packages. The hydrodynamic radius is calculated by averaging six replicates each containing 10 measurements with an acquisition time of 1 s, with the complexes suspended in nanopure water.

Cell Transfection. Chinese hamster ovary cells, cultured at 37 °C with 5% CO_2 in Alpha's modified Eagle's medium (a-MEM-5523) (Sigma) supplemented with addition of 10% cosmic calf serum (Hyclone), were plated at 30 000 cells/cm^2 in 10 cm^2 optical dishes of 1.5 coverglass treated with poly-L-lysine (MatTec Corp). Cellular transfection was carried out 24 h after plating. Medium was exchanged after 24 h of transfection to remove any unreacted AuNP complex. Cell viability was verified using Trypan blue exclusion test of cell viability after 24 h, in addition to visual conformation on the microscope to assess the cell health. No evidence of chromosomal condensation or changes in cell morphology was observed following transfection, indicative of no cytotoxicity at the transfection agent concentrations employed in this study. Trypan blue assays confirmed that cell viability was maintained at 90% following transfection for all experiments relative to control cells. Cell division was occurring over the time span of the experiment, with a doubling rate of 2% per hour, resulting in confluence at 48 h. Due to confluence affecting cell growth behavior, the experimental data were limited to 24 h measurements. Experiments were conducted in triplicate.

Optical Microscopy. Confocal microscopy images were obtained on a Nikon Eclipse Ti inverted microscope at 20× magnification. Samples were excited using a Yokogawa automated 5000 rpm spinning disk confocal microscope equipped with lasers to excite the DyLight350 (405 nm, 1 s exposure), DyLight488 (488 nm, 300 ms exposure), and mCherry (561 nm, 200 ms exposure). Images were collected by an Andor Clara high-resolution CCD at 20×. Measurements were taken at 30 min intervals for 24 h while incubated in a stage-mounted live-cell chamber, kept in focus by a Nikon Perfect Focus system. Images were analyzed for total intensity and cell number by ImageJ software. Intracellular release kinetics were monitored by tracking DyLight intensities normalized to cell count. The *Z*-contrast scanning spectral confocal microscopy images were obtained on a Nikon Eclipse Ti C1 spectral confocal inverted microscope at 60× oil magnification. Cells were stained for surface membrane with AlexaFluor594-labeled wheatgerm agglutinin (WGA594, Life Technologies) and nucleus with 4′,6-diamidino-2-phenylindole dihydrochloride (DAPI, Sigma). A new cell dish was used for each time point, due to the effects of staining on cell health over time.

Image Analysis. The kinetics of the images were analyzed with ImageJ software, using a standard rolling ball radius of 50 pixels to subtract the background to remove any cellular autofluorescence, and the total intensity of each image was measured per time frame. The resulting intensity was corrected for cell count and plotted to an exponential one-phase model, to fit the first-order association kinetics of the release of the sdDNA and plasmid from the surface of the AuNP, plotted with standard deviation of the samples. Each experimental trial was imaged in eight separate regions of the cell dish per time point, with $n = 3$ per sample. The plots were analyzed for differences using the student's unpaired *t* test to determine statistical differences in the samples. Protein expression was analyzed with ImageJ, and measured fluorescence was corrected to cell count per time fame.

Conflict of Interest: The authors declare no competing financial interest.

Acknowledgment. We wish to thank S. Hira for helpful discussions on imaging approaches to monitor live-cell responses. Support for this work was provided by the Florida State University through a FSU-planning grant.

Supporting Information Available: Gel electrophoresis, DLS data, the control live-cell microscopy of independent nucleic acid release, videos of the 24 h time points, the mCherry expression profiles for the controls, and synthetic sequence information. This material is available free of charge *via* the Internet at http://pubs.acs.org.

REFERENCES AND NOTES

1. Glover, D. J.; Lipps, H. J.; Jans, D. A. Towards Safe, Non-viral Therapeutic Gene Expression in Humans. *Nat. Rev. Genet.* **2005**, *6*, 299–310.
2. Hsu, C. Y. M.; Uludag, H. Cellular Uptake Pathways of Lipid-Modified Cationic Polymers in Gene Delivery to Primary Cells. *Biomaterials* **2012**, *33*, 7834–7848.
3. Liu, F.; Huang, L. Development of Non-viral Vectors for Systemic Gene Delivery. *J. Controlled Release* **2002**, *78*, 259–266.
4. Pouton, C. W.; Seymour, L. W. Key Issues in Non-viral Gene Delivery. *Adv. Drug Delivery Rev.* **2001**, *46*, 187–203.
5. Vijayanathan, V.; Thomas, T.; Thomas, T. J. DNA Nanoparticles and Development of DNA Delivery Vehicles for Gene Therapy. *Biochemistry* **2002**, *41*, 14085–14094.

6. Mintzer, M. A.; Simanek, E. E. Nonviral Vectors for Gene Delivery. *Chem. Rev.* **2009**, *109*, 259–302.
7. Zhang, Y.; Satterlee, A.; Huang, L. *In Vivo* Gene Delivery by Nonviral Vectors: Overcoming Hurdles?. *Mol. Ther.* **2012**, *20*, 1298–1304.
8. Pissuwan, D.; Niidome, T.; Cortie, M. B. The Forthcoming Applications of Gold Nanoparticles in Drug and Gene Delivery Systems. *J. Controlled Release* **2011**, *149*, 65–71.
9. Parak, W. J.; Pellegrino, T.; Plank, C. Labelling of Cells with Quantum Dots. *Nanotechnology* **2005**, *16*, R9–R25.
10. Park, J. S.; Na, K.; Woo, D. G.; Yang, H. N.; Kim, J. M.; Kim, J. H.; Chung, H. M.; Park, K. H. Non-viral Gene Delivery of DNA Polyplexed with Nanoparticles Transfected into Human Mesenchymal Stem Cells. *Biomaterials* **2010**, *31*, 124–32.
11. Dorasamy, S.; Narainpersad, N.; Singh, M.; Ariatti, M. Novel Targeted Liposomes Deliver siRNA to Hepatocellular Carcinoma Cells *in Vitro*. *Chem. Biol. Drug Des.* **2012**, *80*, 647–656.
12. Tian, W. D.; Ma, Y. Q. Insights into the Endosomal Escape Mechanism *via* Investigation of Dendrimer−Membrane Interactions. *Soft Matter* **2012**, *8*, 6378–6384.
13. Wang, T.; Upponi, J. R.; Torchilin, V. P. Design of Multifunctional Non-viral Gene Vectors To Overcome Physiological Barriers: Dilemmas and Strategies. *Int. J. Pharm.* **2012**, *427*, 3–20.
14. Rosi, N. L.; Giljohann, D. A.; Thaxton, C. S.; Lytton-Jean, A. K.; Han, M. S.; Mirkin, C. A. Oligonucleotide-Modified Gold Nanoparticles for Intracellular Gene Regulation. *Science* **2006**, *312*, 1027–1030.
15. Seferos, D. S.; Prigodich, A. E.; Giljohann, D. A.; Patel, P. C.; Mirkin, C. A. Polyvalent DNA Nanoparticle Conjugates Stabilize Nucleic Acids. *Nano Lett.* **2009**, *9*, 308–311.
16. Rejman, J.; Tavernier, G.; Bavarsad, N.; Demeester, J.; De Smedt, S. C. mRNA Transfection of Cervical Carcinoma and Mesenchymal Stem Cells Mediated by Cationic Carriers. *J. Controlled Release* **2010**, *147*, 385–391.
17. Akinc, A.; Langer, R. Measuring the pH Environment of DNA Delivered Using Nonviral Vectors: Implications for Lysosomal Trafficking. *Biotechnol. Bioeng.* **2002**, *78*, 503–508.
18. Nel, A. E.; Mädler, L.; Velegol, D.; Xia, T.; Hoek, E. M.; Somasundaran, P.; Klaessig, F.; Castranova, V.; Thompson, M. Understanding Biophysicochemical Interactions at the Nano-Bio Interface. *Nat. Mater.* **2009**, *8*, 543–557.
19. Chou, L.; Ming, K.; Chan, W. Strategies for the Intracellular Delivery of Nanoparticles. *Chem. Soc. Rev.* **2011**, *40*, 233–245.
20. Ochs, M.; Carregal-Romero, S.; Rejman, J.; Braeckmans, K.; De Smedt, S. C.; Parak, W. J. Light-Addressable Capsules as Caged Compound Matrix for Controlled Triggering of Cytosolic Reactions. *Angew. Chem., Int. Ed.* **2013**, *52*, 695–699.
21. Bell, P. C.; Bergsma, M.; Dolbnya, I. P.; Bras, W.; Stuart, M. C. A.; Rowan, A. E.; Feiters, M. C.; Engberts, J. Transfection Mediated by Gemini Surfactants: Engineered Escape from the Endosomal Compartment. *J. Am. Chem. Soc.* **2003**, *125*, 1551–1558.
22. Pittella, F.; Zhang, M.; Lee, Y.; Kim, H. J.; Tockary, T.; Osada, K.; Ishii, T.; Miyata, K.; Nishiyama, N.; Kataoka, K. Enhanced Endosomal Escape of siRNA-Incorporating Hybrid Nanoparticles from Calcium Phosphate and PEG-Block Charge-Conversional Polymer for Efficient Gene Knockdown with Negligible Cytotoxicity. *Biomaterials* **2011**, *32*, 3106–3114.
23. Varkouhi, A. K.; Scholte, M.; Storm, G.; Haisma, H. J. Endosomal Escape Pathways for Delivery of Biologicals. *J. Controlled Release* **2011**, *151*, 220–228.
24. Felgner, P. L.; Gadek, T. R.; Holm, M.; Roman, R.; Chan, H. W.; Wenz, M.; Northrop, J. P.; Ringold, G. M.; Danielsen, M. Lipofection: A Highly Efficient, Lipid-Mediated DNA-Transfection Procedure. *Proc. Natl. Acad. Sci. U.S.A.* **1987**, *84*, 7413–7417.
25. Patil, S. D.; Rhodes, D. G.; Burgess, D. J. DNA-Based Therapeutics and DNA Delivery Systems: A Comprehensive Review. *AAPS J.* **2005**, *7*, E61–E77.
26. Bauhuber, S.; Hozsa, C.; Breunig, M.; Gopferich, A. Delivery of Nucleic Acids *via* Disulfide-Based Carrier Systems. *Adv. Mater.* **2009**, *21*, 3286–3306.
27. Muroski, M. E.; Kogot, J. M.; Strouse, G. F. Bimodal Gold Nanoparticle Therapeutics for Manipulating Exogenous and Endogenous Protein Levels in Mammalian Cells. *J. Am. Chem. Soc.* **2012**, *134*, 19722–19730.
28. Kong, W. H.; Bae, K. H.; Jo, S. D.; Kim, J. S.; Park, T. G. Cationic Lipid-Coated Gold Nanoparticles as Efficient and Non-cytotoxic Intracellular siRNA Delivery Vehicles. *Pharm. Res.* **2013**, *29*, 362–374.
29. Rhim, W.-K.; Kim, J.-S.; Nam, J.-M. Lipid−Gold-Nanoparticle Hybrid-Based Gene Delivery. *Small* **2008**, *4*, 1651–1655.
30. Lim, Y. B.; Kim, S. M.; Suh, H.; Park, J. S. Biodegradable, Endosome Disruptive, and Cationic Network-Type Polymer as a Highly Efficient and Nontoxic Gene Delivery Carrier. *Bioconjugate Chem.* **2002**, *13*, 952–957.
31. Moore, N. M.; Sheppard, C. L.; Barbour, T. R.; Sakiyama-Elbert, S. E. The Effect of Endosomal Escape Peptides on *In Vitro* Gene Delivery of Polyethylene Glycol-Based Vehicles. *J. Gene Med.* **2008**, *10*, 1134–1149.
32. Scott, C. C.; Gruenberg, J. Ion Flux and the Function of Endosomes and Lysosomes: pH Is Just the Start. *BioEssays* **2011**, *33*, 103–110.
33. Suh, J.; An, Y.; Tang, B. C.; Dempsey, C.; Huang, F. R.; Hanes, J. Real-Time Gene Delivery Vector Tracking in the Endo-Lysosomal Pathway of Live Cells. *Microsc. Res. Technol.* **2012**, *75*, 691–697.
34. Ghosh, P.; Han, G.; De, M.; Kim, C. K.; Rotello, V. M. Gold Nanoparticles in Delivery Applications. *Adv. Drug Delivery Rev.* **2008**, *60*, 1307–1315.
35. Sandhu, K. K.; Mcintosh, C. M.; Simard, J. M.; Smith, S. W.; Rotello, V. M. Gold Nanoparticle-Mediated Transfection of Mammalian Cells. *Bioconjugate Chem.* **2002**, *13*, 3–6.
36. Hong, R.; Han, G.; Fernández, J. M.; Kim, B. J.; Forbes, N. S.; Rotello, V. M. Glutathione-Mediated Delivery and Release Using Monolayer Protected Nanoparticle Carriers. *J. Am. Chem. Soc.* **2006**, *128*, 1078–1079.
37. Zhu, Z. J.; Tang, R.; Yeh, Y. C.; Miranda, O. R.; Rotello, V. M.; Vachet, R. W. Determination of the Intracellular Stability of Gold Nanoparticle Monolayers Using Mass Spectrometry. *Anal. Chem.* **2012**, *84*, 4321–4326.
38. Jennings, T. L.; Singh, M. P.; Strouse, G. F. Fluorescent Lifetime Quenching near $D = 1.5$ nm Gold Nanoparticles: Probing NSET Validity. *J. Am. Chem. Soc.* **2006**, *128*, 5462–5467.
39. Yun, C. S.; Javier, A.; Jennings, T.; Fisher, M.; Hira, S.; Peterson, S.; Hopkins, B.; Reich, N. O.; Strouse, G. F. Nanometal Surface Energy Transfer in Optical Rulers, Breaking the FRET Barrier. *J. Am. Chem. Soc.* **2005**, *127*, 3115–3119.
40. Prigodich, A. E.; Randeria, P. S.; Briley, W. E.; Kim, N. J.; Daniel, W. L.; Giljohann, D. A.; Mirkin, C. A. Multiplexed Nanoflares: mRNA Detection in Live Cells. *Anal. Chem.* **2012**, *84*, 2062–2066.
41. Armstrong, R. E.; Strouse, G. F. Rationally Manipulating Aptamer Binding Affinities in a Stem-Loop Molecular Beacon. *Bioconjugate Chem.* **2014**, *25*, 1769–1776.
42. Sperling, R. A.; Gil, P. R.; Zhang, F.; Zanella, M.; Parak, W. J. Biological Applications of Gold Nanoparticles. *Chem. Soc. Rev.* **2008**, *37*, 1896–1908.
43. Tantra, R.; Knight, A. Cellular Uptake and Intracellular Fate of Engineered Nanoparticles: A Review on the Application of Imaging Techniques. *Nanotoxicology* **2011**, *5*, 381–392.
44. Dempsey, G. T.; Vaughan, J. C.; Chen, K. H.; Bates, M.; Zhuang, X. Evaluation of Fluorophores for Optimal Performance in Localization-Based Super-resolution Imaging. *Nat. Methods* **2011**, *8*, 1027–1036.
45. Muroski, M. E.; Morgan, T. J.; Levenson, C. W.; Strouse, G. F. A Gold Nanoparticle Pentapeptide: Gene Fusion To Induce Targeted Gene Expression in Mesenchymal Stem Cells. *J. Am. Chem. Soc.* **2014**, *136*, 14763–14767.
46. Oh, E.; Susumu, K.; Goswami, R.; Mattoussi, H. One-Phase Synthesis of Water-Soluble Gold Nanoparticles with Control Over Size and Surface Functionalities. *Langmuir* **2010**, *26*, 7604–7613.

47. Maurisse, R.; De Semir, D.; Emamekhoo, H.; Bedayat, B.; Abdolmohammadi, A.; Parsi, H.; Gruenert, D. C. Comparative Transfection of DNA into Primary and Transformed Mammalian Cells from Different Lineages. *BMC Biotechnol.* **2010**, *10*, 1–9.
48. Woehrle, G. H.; Brown, L. O.; Hutchison, J. E. Thiol-Functionalized, 1.5-nm Gold Nanoparticles through Ligand Exchange Reactions: Scope and Mechanism of Ligand Exchange. *J. Am. Chem. Soc.* **2005**, *127*, 2172–2183.
49. Dalby, B.; Cates, S.; Harris, A.; Ohki, E. C.; Tilkins, M. L.; Price, P. J.; Ciccarone, V. C. Advanced Transfection with Lipofectamine 2000 Reagent: Primary Neurons, siRNA, and High-Throughput Applications. *Methods* **2004**, *33*, 95–103.